Molecular Dynamics Study on the Interactions of Porphyrin with Two Antiparallel Human Telomeric Quadruplexes

ARTICLE *in* THE JOURNAL OF PHYSICAL CHEMISTRY B · MAY 2010

Impact Factor: 3.3 · DOI: 10.1021/jp101373p · Source: PubMed

3 AUTHORS, INCLUDING:

Minghui Li
National Institutes of Health
14 PUBLICATIONS **102** CITATIONS

Molecular Dynamics Study on the Interactions of Porphyrin with Two Antiparallel Human Telomeric Quadruplexes

Ming-Hui Li, Quan Luo, and Ze-Sheng Li*

Institute of Theoretical Chemistry, State Key Laboratory of Theoretical and Computational Chemistry, Jilin University, Changchun 130023, People's Republic of China

Received: February 13, 2010; Revised Manuscript Received: April 2, 2010

We investigated the binding interactions of a porphyrin derivative (TMPyP4) with two antiparallel basket-type human telomeric quadruplexes under K^+ ion conditions by molecular dynamics simulations. Nine quadruplex−TMPyP4 complexes each with a 1:1 stoichiometry were built for every quadruplex, including the binding modes of end stacking, intercalation, external groove binding, and external loop stacking. Detailed structures analysis, free energy calculations, and principal components analysis were performed. The results show that the end stacking mode is the best binding mode, with high binding affinity and high stability of quadruplexes, and next is the external loop stacking mode, with relatively high binding affinity and high stability of quadruplexes. The groove binding mode has the relatively low binding affinity, and the quadruplexes are stabilized well. The intercalation mode has very high binding affinity, but the quadruplexes are not stabilized and show very high flexibility.

Introduction

Human telomeric DNA has a single-strand segment overhanging at the end of its double-strand DNA helix consisting of tandem repeats of the sequence d(TTAGGG).[1,2] These G-rich overhangs can form four-stranded structures called G-quadruplexes (G4) that are built of stacked G-tetrads each containing the planar association of four guanine nucleobases in a stable Hoogsteen hydrogen-bonding arrangement in the presence of monovalent cations such as potassium cation (K^+) or sodium cation (Na^+).[3–5] The formation of the G4 structures can effectively inhibit the activity of the telomerase,[6] an enzyme that is critical for the proliferation of cancer cells.[7] Therefore, intense interest has arisen recently in searching for effective small molecules that are capable of inducing and stabilizing the G4 structure to be potential anticancer agents.

A number of G-quadruplex-binding compounds have been identified.[8–11] Cationic *meso*-tetrakis(4-(*N*-methylpyridiumyl))porphyrin (TMPyP4) has been of particular interest since it can inhibit the activity of telomerase upon binding to human telomeric DNA quadruplexes.[12] Extensive investigations have been undertaken to determine the structures of quadruplex−TMPyP4 complexes, the binding modes, and the binding stoichiometries.[13–18] Several different modes of TMPyP4 binding to quadruplexes have been proposed, including end stacking on the G-quartets, intercalative binding between adjacent G-quartets, outside groove binding, and external loop stacking, but few studies addressed all the possible binding kinds simultaneously. For example, Hurley and co-workers proposed that TMPyP4 molecules bind to the end-loops of the antiparallel G-quadruplex structure through external stacking based on the spectroscopic methods, photocleavage experiments, and molecular dynamics calculations.[15] Haq et al. proposed that TMPyP4 molecules intercalate between two G-tetrads for d(G2T2G2TGTG2T2G2), d(AG3[T2AG3]3), and $[d(T4G4)]_4$ based on isothermal titration calorimetry (ITC), UV−vis absorption spectrometry, and molecular-modeling methods.[16] Recently, Wei et al. reported that TMPyP4 binds to antiparallel G4 by both the end stacking and the intercalation modes.[17] Zhang et al. have recently characterized the binding of TMPyP4 with the human telomeric G-quadruplex under different K^+ concentrations and found the end stacking mode and groove binding mode were presumed mainly by the results of time-resolved fluorescence spectroscopy.[18] The binding stoichiometry of TMPyP4 to human telomeric quadruplex structures did not reach an agreement so far, even for the similar or same quadruplex sequence.

Recently, the conformational conversion of the human telomeric quadruplexes induced by TMPyP4 was also investigated. Zhang et al. found that TMPyP4 can directly induce the formation of the antiparallel G4 structure from the single-strand oligonucleotide $d[TAGGG(TTAGGG)_3T]$ in the absence of K^+ and that it can preferentially transform the hybrid-type quadruplex structure into an antiparallel one in the presence of K^+.[18] A study using ^{125}I-radioprobing for a similar DNA sequence also showed that adding TMPyP4 stabilizes a basket conformation in K^+ solution.[19] The finding was further confirmed by CD studies that TMPyP4 in dilute solution promoted the conversion of the hybrid structures to an antiparallel conformation.[20] An antiparallel basket G-quadruplex conformation was found for the human telomeric $d[AGGG(TTAGGG)_3]$ sequence in Na^+ solution, in which the core is made up of three G-tetrads adjoined by one diagonal and two lateral loops.[21] A new intramolecular human telomeric G-quadruplex conformation formed by the $d[(GGGTTA)_3GGGT]$ sequence in K^+ solution was reported recently, which is an antiparallel-stranded basket-type G-quadruplex involving only two layers of G-tetrads.[22]

To date, only two atomic structures for quadruplex−TMPyP4 complexes were obtained. One is formed between a parallel-stranded bimolecular human telomeric quadruplex and TMPyP4 by the external loop stacking mode.[13] The other is formed between a parallel-stranded G-quadruplex in the *c-myc* promoter region and TMPyP4 by the end stacking mode.[23] The rational design of G-quadruplex-binding drugs requires knowledge of the detailed structures of their ligand complexes to be helpful.

* Corresponding author. E-mail: zeshengli@hit.edu.cn.

10.1021/jp101373p
Published on Web 04/20/2010

It is necessary to implement detailed research on the interactions between the TMPyP4 and human telomeric G-quadruplexes involving all of the binding modes.

Therefore, in the present work, molecular dynamics (MD) simulation studies were performed to investigate the interactions between two antiparallel basket-type Tel-21 (d[(GGGTTA)$_3$GGG]) quadruplexes and TMPyP4 in the presence of K^+ ions. The two Tel-21 quadruplexes have three G-quartet layers and two G-quartet layers, respectively. Nine quadruplex−TMPyP4 complexes each with a 1:1 stoichiometry were obtained for every quadruplex, containing all binding modes. Then, the structure and stability of the complexes were analyzed in detail. To characterize the energetics of the quadruplex−TMPyP4 interactions and to predict the most effective TMPyP4-binding modes, the absolute free energy and the binding free energy were estimated. Principal components analysis was performed to describe the dynamic effects of the ligand TMPyP4 on the quadruplex structures. So this is an exhaustive study to provide detailed insight into the binding interactions between TMPyP4 and two antiparallel G-quadruplex structures.

Methods

Model Generation. Two experimental structures of G-quadruplexes were chosen as starting models: (i) unimolecular antiparallel basket-type G-quadruplex with three stacked G-tetrads which are connected by two lateral loops and a central diagonal loop (PDB code 143D)[21] and (ii) unimolecular antiparallel basket-type G-quadruplex with only two stacked G-tetrads which are connected by two lateral loops and a central diagonal loop (PDB code 2KF8).[22] For comparison between the two conformations, in each of them we removed the terminal nucleotide. We manually placed two K^+ ions in the central cavities of 143D and one K^+ ion in the central cavity of 2KF8 using INSIGHTII software.[24] The presence and nature of the coordinated ions are very important to the stability of the G-quadruplexes, and the absence of coordinated cations remarkably modifies the original structure and causes evident deformations or disruption.[25] The larger the ion size is ($Li^+ < Na^+ < K^+$), the more the regular quadruplex conformation is maintained, and K^+ is demonstrated to be the most efficient to stabilize the G-quadruplexes.[25–28]

The initial molecular model of TMPyP4 is based on the X-ray crystal structure at 2.09 Å resolution.[13] Then it was optimized with Gaussian03 software, and partial charges were derived using the HF/6-31G* basis set followed by RESP calculation in an antechamber module of Amber 10 software.[29] The remaining parameters for TMPyP4 were obtained from the generalized amber forcefield (GAFF).[30]

Docking. The optimized structure of TMPyP4 was manually docked into the binding sites of end stacking, intercalation, external groove binding, and external loop stacking in the two antiparallel quadruplexes (Figure 1), based on the experimental reports.[15–18] The intercalation complexes were built by increasing the distance between two consecutive G-tetrads and then inserting TMPyP4 into the sites, simultaneously, removing the potassium ions that occupied the sites of the entrance of TMPyP4. The distance between two consecutive tetrads is increased to 5.4 Å, which can make the initial modeling structures of the intercalation mode more reasonable. Cavallari et al. found the insertion of a porphyrin induces a significant separation between the adjacent tetrads.[31] The Raman hyperchromicities and shifts indicated that the intercalative TMPyP4 can lengthen the vertical distance between adjacent G-tetrads

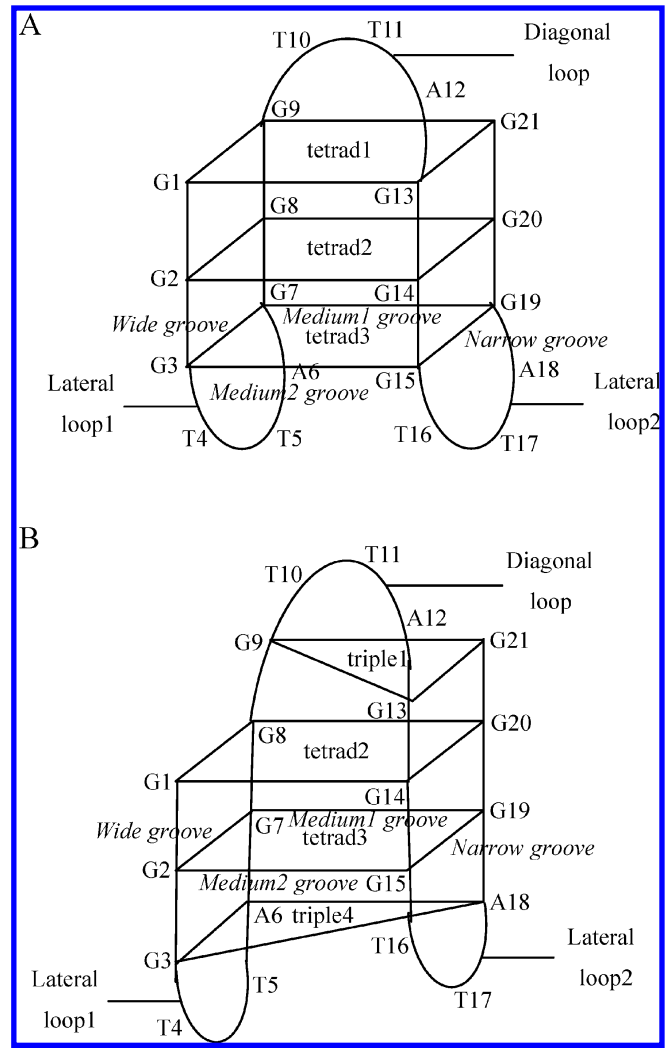

Figure 1. Sketch of two antiparallel basket-type G-quadruplex structures, 143D (A) and 2KF8 (B).

of $AG_3(T_2AG_3)_3$.[17] Some reports suggested that the presence of K^+ in the space between the G-tetrads prevents intercalation of aromatic molecules into G-quadruplexes by steric hindrance and electrostatic repulsion.[31,32] The positions and orientations of TMPyP4 in the end stacking, external groove binding, and external loop stacking complexes were optimized through a flexible docking approach using the AFFINITY module of INSIGHTII. During external groove binding processes, the quadruplex structures were restrained to their original positions and the TMPyP4 atoms movable, while the loop nucleotides of the quadruplex contacted with ligand were also movable during the end stacking and external loop stacking processes. As a result, a number of possible conformations were evaluated. Finally, the lowest-energy conformation for each site was chosen as a starting model. Hence, 18 1:1 quadruplex−TMPyP4 complexes were obtained. Their nomenclature and descriptions are provided in Table 1.

MD Simulations. All models including two quadruplexes and quadruplex−TMPyP4 complexes were neutralized by adding K^+ ions and immersed in truncated octahedral boxes of TIP3P[33] water molecules extending up to 9 Å[34] from the solute in each direction. These systems were then optimized and equilibrated using multiple initial minimization and dynamics runs. First, the solute and inner K^+ ions within the quadruplex were fixed, respectively, with force constants of 500, 100, and 10 kcal/molÅ^2 in a set of subsequent 4000-step minimizations. Then, a

TABLE 1: List of All Simulations Performed in This Article

model name	structure	time (ns)
143D	three-G-tetrad G-Quadruplex	20
A-1	end stacking with TMPyP4 residing between the diagonal loop and tetrad1	20
A-2	end stacking with TMPyP4 residing between the two lateral loops and tetrad3	20
A-3	intercalation with TMPyP4 residing between the tetrad1 and tetrad2	20
A-4	intercalation with TMPyP4 residing between the tetrad2 and tetrad3	20
A-5	external groove binding with TMPyP4 residing in the wide groove	20
A-6	external groove binding with TMPyP4 residing in the narrow groove	20
A-7	external groove binding with TMPyP4 residing in the medium1 groove	30
A-8	external groove binding with TMPyP4 residing in the medium2 groove	20
A-9	external loop stacking with TMPyP4 interacting with the lateral loops	20
2KF8	two-G-tetrad G-Quadruplex	20
B-1	end stacking with TMPyP4 residing between the diagonal loop and triple1	20
B-2	end stacking with TMPyP4 stacked on the tetrad2	20
B-3	end stacking with TMPyP4 stacked on the tetrad3	25
B-4	intercalation with TMPyP4 residing between the tetrad2 and tetrad3	20
B-5	external groove binding with TMPyP4 residing in the wide groove	20
B-6	external groove binding with TMPyP4 residing in the narrow groove	20
B-7	external groove binding with TMPyP4 residing in the medium1 groove	35
B-8	external groove binding with TMPyP4 residing in the medium2 groove	20
B-9	external loop stacking with TMPyP4 interacting with the lateral loops	30

4000-step full minimization was carried out for the entire systems. The systems were then heated to 298 K over 50 ps at constant volume with a force constant of 50 kcal/mol$Å^2$ maintained for the solute and inner ions and followed by a set of MD simulations similar to the restrained minimizations; i.e., the solute and inner ions were restrained by 50, 40, 30, 20, and 10 kcal/mol$Å^2$ force constants in a set of subsequent 50 ps restrained MD simulations. The final stage of equilibration involved a 500 ps run using a low 5 kcal/mol$Å^2$ constraint on the solute and inner ions. The systems were then subject to a 20−35 ns unconstrained MD simulation (details are provided in Table 1). All MD simulations were performed in the isothermic−isobaric ensemble ($T = 298$ K, $P = 1$ atm). The particle mesh Ewald (PME) method[35] of calculating long-range electrostatic interactions was employed with a cutoff of 10 Å. SHAKE[36] was applied to constrain the bonds containing hydrogen, which allowed us to use a 2 fs time step. Simulations were performed with the parm99bsc0 force field[37] using the SANDER module in the AMBER10.0 package.

Free Energy Calculations. Free energies were calculated using the MM_PBSA method that combines the molecular mechanical energies with the continuum solvent approaches by the programs in the AMBER10.0. The molecular mechanical energies are determined with the Sander program from AMBER. The electrostatic contribution to the solvation free energy is calculated with the PBSA program.[38] The nonpolar contribution to the solvation free energy is computed with the MOLSURF program.[39] The 500 snapshots for the quadruplex−TMPyP4 complexes from the last 10 ns of the trajectories at 20 ps intervals were used for energetic analysis. The K^+ ions in the central channel of the G-quadruplexes were included for free energy calculations to obtain meaningful results.[40] The solute entropic contribution was estimated with the NMODE module in AMBER, using snapshots collected every 200 ps.

Principal Components Analysis. Reducing the dimensionality of the data obtained from molecular dynamics simulations can help in identifying configurational space that contains only a few degrees of freedom in which anharmonic motion occurs. Principal components analysis (PCA) is a powerful tool to separate large-scale correlated motions from local harmonic fluctuations.[41,42] To eliminate translation and rotation motions and isolate only the internal motions of the system, each frame of the trajectory was fit to the starting structure. The configurational space was constructed using a simple linear transformation in Cartesian coordinate to produce a $3N \times 3N$ covariance matrix. The covariance matrix was then diagonalized to obtain a set of eigenvectors and corresponding eigenvalues, which represented the directions of motion and the amount of motion along each eigenvector, respectively.[43]

Results and Discussion

Three-G-Tetrad G-Quadruplex and Its Complexes with TMPyP4. The root-mean-square deviation (rmsd) can be used as a measure of the conformational stability of a structure during the simulation.[41] Figure 2 displays the rmsd values of all atoms (black) and G-tetrads (red) for the 143D system, with the starting modeling structure as a reference point. The rmsd trajectory of all atoms becomes stable after about 7.5 ns, with the rmsd values ∼2.4 Å, but a protuberance is shown between 12.5 and 15.0 ns. Investigation of the simulation trajectory shows that the T4 base displays very high flexibility during 12.5−15.0 ns. The G-tetrads are very rigid and show low rmsd value of ∼1.1 Å, due to the strong H-bonds and stacking interactions within the G-tetrads. The average structure of 143D over the last 10 ns simulation is shown in Figure 3A, with two K^+ ions coordinated in the central cavity. The loops are preserved well, and a triple plane consisting of T5, A6, and A18 is formed at the bottom of

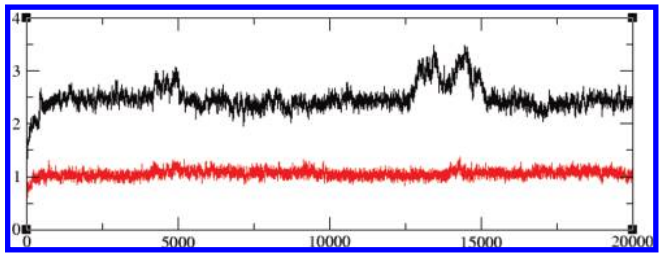

Figure 2. rmsd values (Å) (*y*-axis) of all atoms (black) and the G-tetrads (red) for the 143D system versus simulation time (ps) (*x*-axis) with the experimental structure as a reference point.

the tetrad3. The distribution of the H-bonds in the average structure is the same as that in the NMR structure, with 22 Hoogsteen hydrogen bonds in the three G-tetrads and four bifurcated hydrogen bonds formed between two bases of tetrad2.

The rmsd trajectories of all atoms (black), G-quadruplex (red), and the G-tetrads (green) for two end stacking complexes of A-1 and A-2 are shown in Figure S1A and S1B in the Supporting Information, with initial docking structures as references. All the rmsd trajectories of A-1 and A-2 become very stable after 9 ns, and all atoms show almost the same rmsd value with the G-quadruplex for both complexes, indicating the ligands are preserved well in each site. The average structures of A-1 and A-2 over the last 10 ns simulations are shown in Figure 3B and 3C, respectively. Since the planar ring of the porphyrin is smaller than a G-tetrad, the ligand is offset so that two 4-methylpyridinium groups effectively protrude into adjacent groove conduits of the quadruplex. As a consequence, the two other substituent rings do not extend as far into their respective DNA grooves and are drawn toward the loop bases. The diagonal loop in A-1 is altered largely, with A12 rotated away from tetrad1 and T11 shifted to stack with the TMPyP4. Two lateral loops are preserved well, with a triple plane formed by T5, A6, and A18. As for A-2, the diagonal loop is retained well, and the two lateral loops show large flexibility, with T4 shifted to stack with the 4-methylpyridinium group in the medium2 groove and A18 to stack with the porphyrin core. The G-tetrads of both models are very rigid, with all the H-bonds retained.

All the rmsd trajectories of A-4 are very stable after 2.5 ns (Figure S1D, Supporting Information), and the rmsd trajectories of A-3 show relatively large fluctuations (Figure S1C, Supporting Information). The ligands in A-3 and A-4 are retained in the initial sites, due to almost the same rmsd values between all atoms and the G-quadruplex. The average structures over the last 10 ns simulation are shown in the Figure 3D and 3E. In the A-3 complex, the G1 and G21 bases move out of the

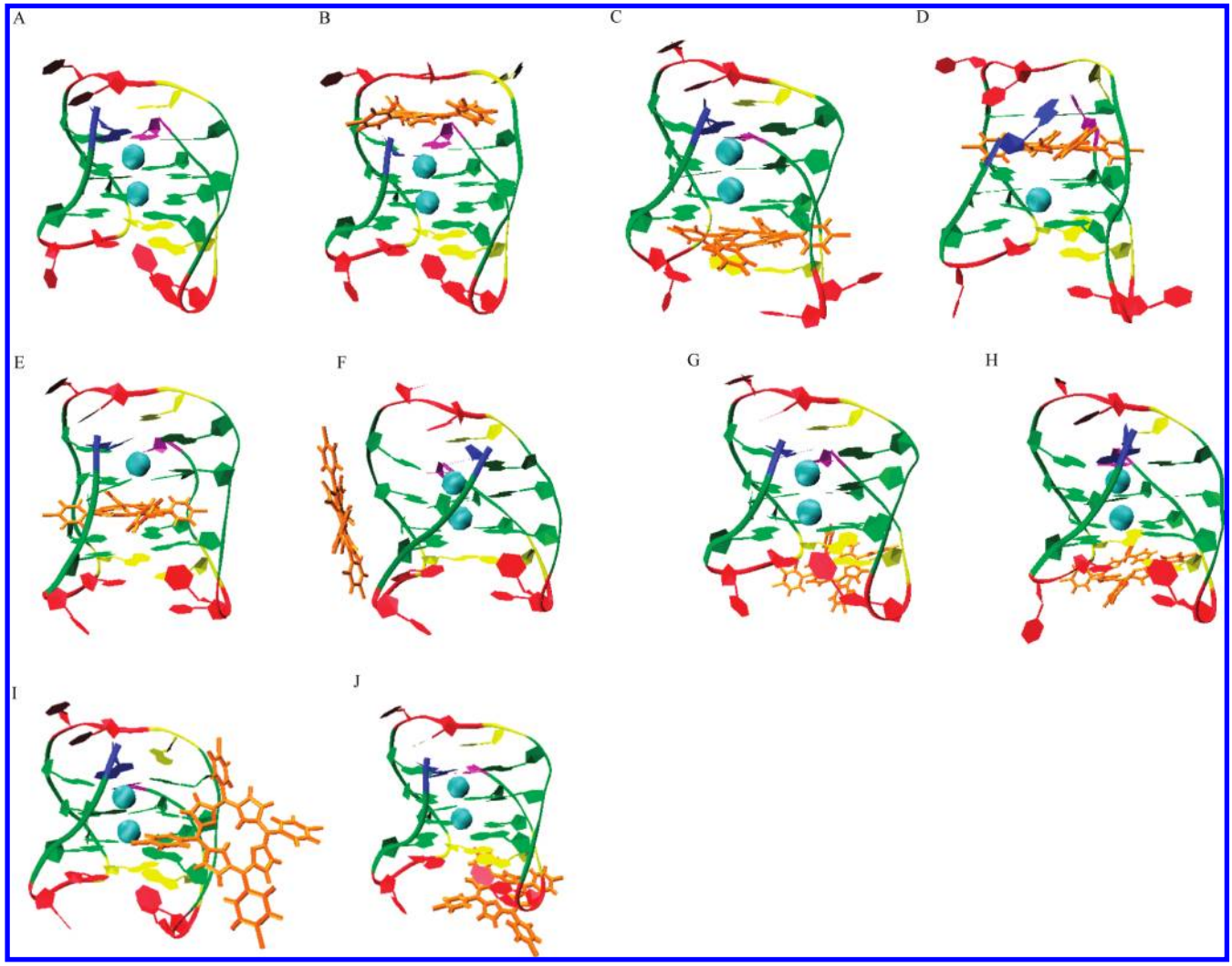

Figure 3. Average structures of 143D (A), A-1 (B), A-2 (C), A-3 (D), A-4 (E), A-5 (F), A-6 (G), A-7 (H), A-8 (I), and A-9 (J). The K^+ ions in the central channel are shown in cyan. The 5′ terminal guanine bases are showed in blue; the 3′ terminal guanine bases are shown in purple; the thymine bases are shown in red; the adenine bases are shown in yellow; and the rest of the guanine bases are shown in green.

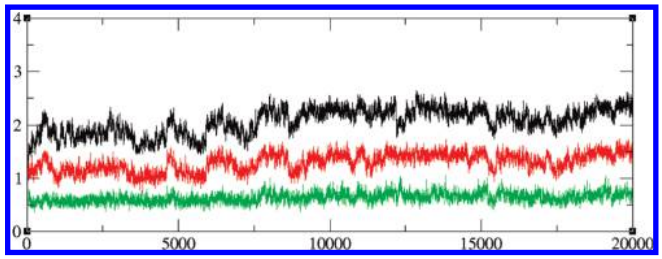

Figure 4. rmsd values (Å) (*y*-axis) of all atoms (black), all planes containing two tetrads and two triples (red), and the G-tetrads (green) for the 2KF8 system versus simulation time (ps) (*x*-axis) with the experimental structure as a reference point.

tetrad1 without forming any H-bonds with other bases. Tetrad2 and tetrad3 of A-3 remain reasonably stable throughout the simulation, with the Hoogsteen hydrogen bonds preserved very well. The conformation of the diagonal loop in A-3 is not preserved, showing T11 interacting with one 4-methylpyridinium group and A12 stacking with G21. Only T5 and A18 of the lateral loops are maintained, stacking at the bottom of the tetrad3. Compared with A-3, the quadruplex structure of A-4 is much more integrated with a better preservation of the tetrads and the loops. All the Hoogsteen hydrogen bonds in the tetrad1 and tetrad2 of A-4 are retained, and eight H-bonds containing only two Hoogsteen hydrogen bonds are formed in the tetrad3. A substituent ring of the TMPyP4 in the A-4 model does not extend as far into its DNA groove, thereby inducing a perturbation of the local planarity of tetrad1 and tetrad2.

Since the size of the TMPyP4 is much larger relative to the size of the grooves, only parts of the TMPyP4 are in the grooves in the initial docking complexes. The rmsd trajectories for A-5 show that TMPyP4 deviates from the initial site at 7.5 ns and then is stabilized during the remaining simulation time (Figure S1E, Supporting Information). During the A-6 simulation, the TMPyP4 leaves the quadruplex to the solvent between 2.6 and 4.0 ns and then comes back to cap on the A6 base steadily (Figure S1F, Supporting Information). As for A-7, the TMPyP4 leaves the initial site to interact with A6 after about 20 ns and then is stabilized at that site until the end (Figure S1G, Supporting Information). All the rmsd trajectories of A-8 are very stable after 7 ns, and TMPyP4 is retained at the initial site relatively well (Figure S1H, Supporting Information). The average structures of A-5, A-6, A-7, and A-8 over the last 10 ns simulations are shown in Figure 3F, 3G, 3H, and 3I, respectively. The ligands in the narrow and medium1 grooves are shifted to interact with the A6 of the lateral loop. For A-5 and A-8, the TMPyP4 molecule interacts with the quadruplex mainly by electrostatic attraction between pyridinium groups and phosphate groups. The G-tetrads of the four models are very rigid and are preserved very well. The loops in the four simulations are also retained well except the A6 base in A-6 and A-7. All the rmsd trajectories of A-9 become very stable after about 2.5 ns, with the TMPyP4 stabilized well on the top of the T17 of the lateral loop2 (Figure S1I, Supporting Information). The average structure over the last 10 ns shows that the G-tetrads and the loops are preserved well (Figure 3J).

Two-G-Tetrad G-Quadruplex and Its Complexes with TMPyP4. Figure 4 displays the rmsd values of all atoms (black), all planes (red), and the G-tetrads (green) for the 2KF8 system, with the starting modeling structure as a reference point. All the rmsd trajectories of 2KF8 become stable after about 10.0 ns, with the rmsd values ~2.3 Å for all atoms, ~1.5 Å for all planes, and ~0.7 Å for the two G-tetrads. Analyzing the simulation trajectory reveals that one K^+ ion is positioned at the midpoint on the top of the G9·G13·G21 triple plane at the beginning of the simulation and remains at that site for the entire simulation. The entry of the K^+ ion can stabilize the triple1 plane. The average structure over the last 10 ns simulation shows that all planes and the loop bases are preserved very well (Figure 5A). There are 23 H-bonds distributed in the average structure, containing 16 Hoogsteen hydrogen bonds in the two tetrads, 4 H-bonds in the triple1, and 3 ones in the triple4.

All the rmsd trajectories of B-1 become very stable after about 10 ns, with the ligand, the G-tetrads, and the triples preserved very well (Figure S2A, Supporting Information). The average structure over the last 10 ns simulation is shown in Figure 5B. The diagonal loop of B-1 is altered largely and shows almost the same conformation as that in A-1, and the two lateral loops are retained. The rmsd trajectories of the B-2 model show that the ligand and two G-tetrads are preserved very well, while the triple planes have a large fluctuation (Figure S2B, Supporting Information). The average structure over the last 7 ns simulation shows that TMPyP4 is stacked with the tetrad1, and the triple1 is disrupted completely (Figure 5C). The G9 and T11 of the diagonal loop are stacked with the TMPyP4, and the triple4 and the two lateral loops are retained. The rmsd trajectories of the B-3 model show that the ligand and two G-tetrads are preserved very well, and the triple planes have a large deviation (Figure S2C, Supporting Information). The average structure over the last 9 ns simulation shows that the TMPyP4 is stacked on the tetrad3 and the triple4 is disrupted (Figure 5D). The triple1 is retained, and the remaining loop bases show high flexibility.

Investigation of the B-4 simulation trajectory finds that the G1 base moves out of the tetrad1 without forming any H-bonds with other bases and displays very high flexibility, which is the main effect to the high fluctuations in the rmsd plots (Figure S2D, Supporting Information). G20 and G21 also move out of the tetrad1 and triple1, respectively, but they show relatively higher rigidity and smaller displacements relative to G1. The average structure is shown in Figure 5E. The triple1 and tetrad1 are disrupted, and the remaining planes and loops are retained well.

The rmsd plots show that the structures of B-5 and B-8 are stable during the whole simulations, and the ligands of them show slight deviations from the initial docking sites (Figure S2E and S2H, Supporting Information). For B-6, TMPyP4 leaves the quadruplex to the solvent and never comes back (Figure S2F, Supporting Information), and so it is not performed for the following analysis. The TMPyP4 in B-7 is stabilized at the initial docking site before 15 ns, but after that it leaves the medium2 groove gradually with only one 4-methylpyridinium group interacting with the quadruplex and shows large flexibility especially after 25 ns (Figure S2G, Supporting Information). The average structures of B-5, B-7, and B-8 over the last 10 ns are shown in Figure 5F, 5G, and 5H, respectively. The quadruplex structures of the three models are preserved very well except the lateral loop1 in B-5. The rmsd trajectories of the B-9 structure become very stable after 16 ns, and the ligand is deviated largely from the initial site (Figure S2I, Supporting Information). The simulation trajectory analysis shows that the TMPyP4 only stacks with T17 before 14 ns, and after that it is shifted to stack with both T17 and T5. The average structure over the last 10 ns is shown in the Figure 5I, from which we can see that the quadruplex conformation is preserved well.

Free Energy Calculations. Free energies obtained using the MM_PBSA methodology can be applied to provide a semi-

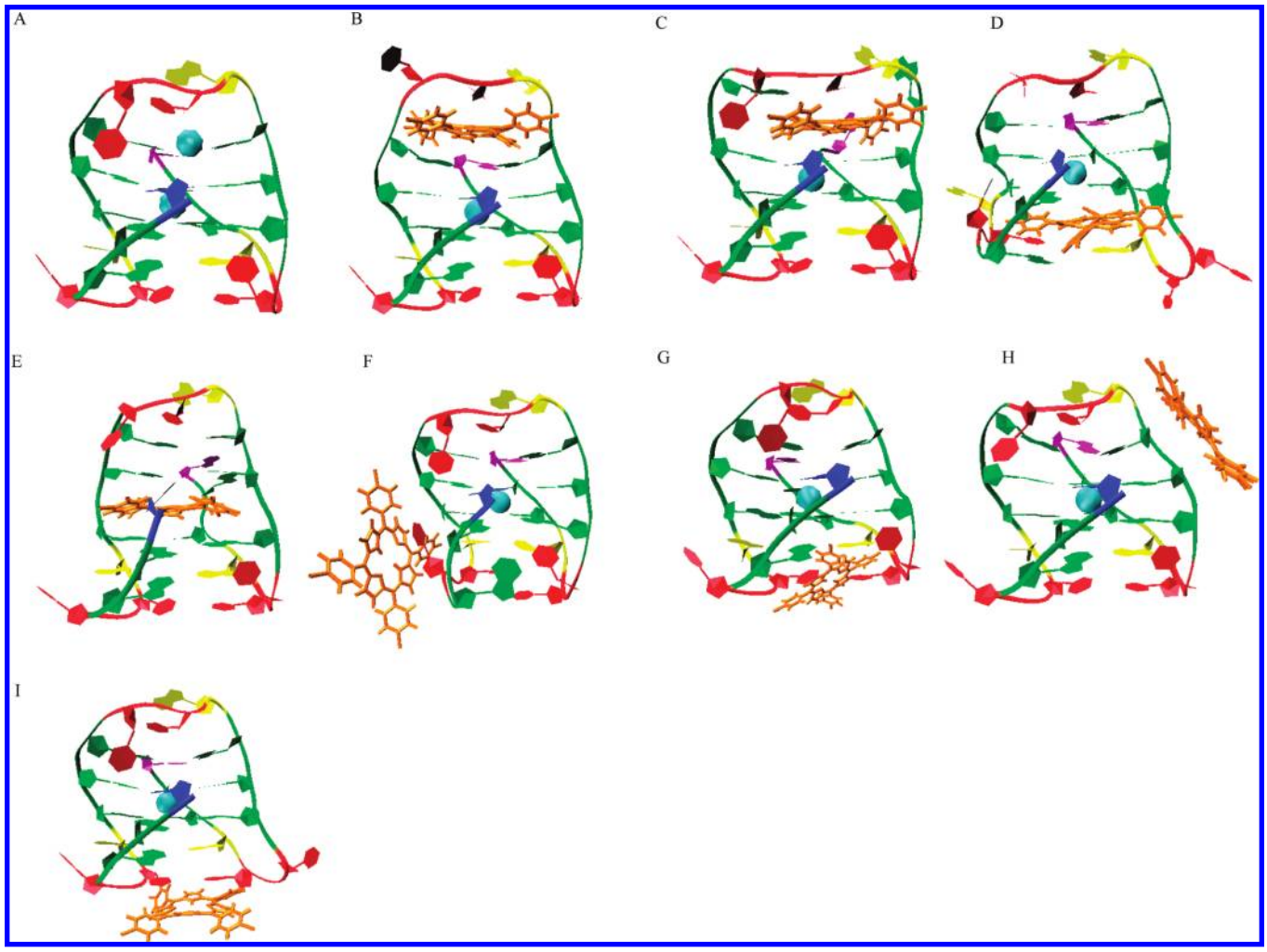

Figure 5. Average structures of 2KF8 (A), B-1 (B), B-2 (C), B-3 (D), B-4 (E), B-5 (F), B-7 (G), B-8 (H), and B-9 (I). The K^+ ions in the central channel are shown in cyan. The 5′ terminal guanine bases are shown in blue, the 3′ terminal guanine bases in purple, the thymine bases in red, the adenine bases in yellow, and the rest of the guanine bases in green.

quantitative estimate of quadruplex model stability and binding affinity with the ligands. The binding free energy components and absolute free energies for 143D−TMPyP4 complexes and 2KF8−TMPyP4 are listed in Table 2 and Table 3, respectively. The total binding free energy is negative for all the complexes, indicating the TMPyP4 can bind to the G-quadruplexes in all the sites of our research. For all complexes, the electrostatic energy (ΔE_{ELEC}) shows tremendously favorable contributions to the total binding free energy, which indicates that the electrostatic attraction interactions between the cationic charges

TABLE 2: Free Energies of 1:1 Three-G-Tetrad Quadruplex−TMPyP4 Complexes[a]

	A-1	A-2	A-3	A-4	A-5	A-6	A-7	A-8	A-9
ΔE_{ELE}	−1738.92	−1838.87	−1895.73	−1944.05	−1581.36	−1487.89	−1546.62	−1571.18	−1511.87
ΔE_{VDW}	−87.39	−94.28	−103.13	−101.22	−29.99	−28.44	−35.14	−33.98	−34.71
ΔE_{INT}	0.00	0.00	0.00	0.00	0.00	0.00	0.00	0.00	0.00
ΔE_{GAS}	−1826.31	−1933.15	−1998.87	−2045.27	−1611.35	−1516.33	−1581.76	−1605.16	−1546.58
ΔE_{PBSUR}	−9.00	−9.44	−9.59	−9.26	−4.67	−3.45	−4.58	−4.45	−4.13
ΔE_{PBCAL}	1767.58	1871.84	1930.92	1973.20	1587.54	1489.50	1543.19	1539.50	1486.86
ΔE_{PBSOL}	1758.59	1862.40	1921.33	1963.93	1582.86	1486.05	1538.60	1535.05	1482.74
ΔE_{PBELE}	28.66	32.97	35.19	29.14	6.18	1.61	−3.44	−31.68	−25.01
ΔE_{PBTOT}	−67.72	−70.75	−77.54	−81.34	−28.49	−30.28	−43.16	−70.11	−63.85
$T\Delta S$	−9.62	−7.98	−6.49	−7.36	−7.72	−5.88	−6.49	−6.71	−6.68
ΔG_{TOT}	−58.1	−62.77	−71.05	−73.98	−20.77	−24.4	−36.67	−63.4	−57.17
ΔE_{PBTOT_COM}	−3877.82	−3868.40	−3766.33	−3783.38	−3868.93	−3874.06	−3882.48	−3913.03	−3906.75
$T\Delta S_{(COM)}$	181.43	181.91	182.32	180.49	180.73	182.06	182.19	181.97	181.23
ΔG_{TOT_COM}	−4059.25	−4050.31	−3948.65	−3963.87	−4049.66	−4056.12	−4064.67	−4095.00	−4087.98

[a] ΔE_{ELE} = Electrostatic energy, ΔE_{VDW} = van der Waals energy, ΔE_{INT} = internal energy, ΔE_{GAS} = total gas phase energy (ΔE_{ELE} + ΔE_{VDW} + ΔE_{INT}), ΔE_{PBSUR} = nonpolar solvation energy, ΔE_{PBCAL} = polar solvation energy, ΔE_{PBSOL} = total solvation energy (ΔE_{PBSUR} + ΔE_{PBCAL}), ΔE_{PBELE} = total electrostatic energy (ΔE_{ELE} + ΔE_{PBCAL}), ΔE_{PBTOT} = enthalpy of binding (ΔE_{GAS} + ΔE_{PBCAL}), $T\Delta S$ = solute entropy for binding, ΔG_{TOT} = binding free energy (ΔE_{PBTOT} − $T\Delta S$), ΔE_{PBTOT_COM} = enthalpy of complex, $T\Delta S_{(COM)}$ = solute entropy of complex, ΔG_{TOT_COM} = absolute free energy of complex. All energy values are in kcal mol^{-1}.

TABLE 3: Free Energies of 1:1 Two-G-Tetrad Quadruplex−TMPyP4 Complexes[a]

	B-1	B-2	B-3	B-4	B-5	B-7	B-8	B-9
ΔE_{ELE}	−1783.47	−1931.11	−2001.26	−2107.71	−1627.70	−1499.99	−1653.46	−1687.62
ΔE_{VDW}	−78.95	−95.33	−101.42	−99.19	−37.11	−16.82	−29.64	−39.28
ΔE_{INT}	0.00	0.00	0.00	0.00	0.00	0.00	0.00	0.00
ΔE_{GAS}	−1862.42	−2026.44	−2102.68	−2206.90	−1664.81	−1516.81	−1683.10	−1726.90
ΔE_{PBSUR}	−7.75	−9.07	−9.77	−9.59	−4.45	−2.45	−3.69	−4.73
ΔE_{PBCAL}	1802.40	1960.88	2034.73	2137.89	1633.37	1495.37	1656.33	1691.98
ΔE_{PBSOL}	1794.65	1951.81	2024.96	2128.29	1628.92	1492.92	1652.64	1687.25
ΔE_{PBELE}	18.93	29.77	33.47	30.18	5.67	−4.62	2.87	4.37
ΔE_{PBTOT}	−67.77	−74.63	−77.72	−78.61	−35.89	−23.89	−30.46	−39.65
$T\Delta S$	−8.87	−7.83	−8.56	−7.21	−8.18	−6.99	−7.58	−6.87
ΔG_{TOT}	−58.9	−66.8	−69.16	−71.4	−27.71	−16.9	−22.88	−32.73
ΔE_{PBTOT_COM}	−3809.44	−3803.03	−3777.54	−3686.04	−3787.30	−3778.28	−3797.22	−3813.80
$T\Delta S_{(COM)}$	181.14	181.21	181.74	180.31	178.98	180.89	180.55	184.40
ΔG_{TOT_COM}	−3990.58	−3984.24	−3959.28	−3866.35	−3966.28	−3959.17	−3977.77	−3998.2

[a] ΔE_{ELE} = Electrostatic energy, ΔE_{VDW} = van der Waals energy, ΔE_{INT} = internal energy, ΔE_{GAS} = total gas phase energy ($\Delta E_{ELE} + \Delta E_{VDW} + \Delta E_{INT}$), ΔE_{PBSUR} = nonpolar solvation energy, ΔE_{PBCAL} = polar solvation energy, ΔE_{PBSOL} = total solvation energy ($\Delta E_{PBSUR} + \Delta E_{PBCAL}$), ΔE_{PBELE} = total electrostatic energy ($\Delta E_{ELE} + \Delta E_{PBCAL}$), ΔE_{PBTOT} = enthalpy of binding ($\Delta E_{GAS} + \Delta E_{PBCAL}$), $T\Delta S$ = solute entropy for binding, ΔG_{TOT} = binding free energy ($\Delta E_{PBTOT} - T\Delta S$), ΔE_{PBTOT_COM} = enthalpy of complex, $T\Delta S_{(COM)}$ = solute entropy of complex, ΔG_{TOT_COM} = absolute free energy of complex. All energy values are in kcal mol^{-1}.

TABLE 4: Eigenvalues (Å^2) of the First Three Eigenvectors for the Three-G-Tetrad Quadruplex and Its Complexes with TMPyP4

	143D	A-1	A-2	A-3	A-4	A-5	A-6	A-7	A-8	A-9
eigenvector1	41.82	19.57	21.69	44.13	25.97	11.86	14.08	42.05	16.53	11.77
eigenvector2	15.06	13.77	8.93	26.03	14.72	10.22	5.93	11.86	13.92	10.82
eigenvector2	9.50	7.06	7.71	13.73	10.58	7.16	5.12	7.53	8.38	8.71

on the pyridinium groups and the anionic charges on the phosphate groups are the largest contributions to the binding of the TMPyP4. The van der Waals energy (ΔE_{VDW}) provides favorable contributions because the porphyrin ring makes vdw contacts with the tetrads and the loops and/or the four 4-methylpyridinium groups also make favorable vdw contacts with the four grooves. The nonpolar solvation energy (ΔE_{SNP}) also presents slightly favorable contributions, while the polar solvation energy (ΔE_{SP}) makes tremendously unfavorable contributions. The resulting balance of the ΔE_{ELEC} and ΔE_{SP} contributions, ΔE_{PBELE}, is unfavorable to the total binding free energy for all systems except A-7, A-8, A-9, and B-7. In addition, unfavorable entropic contribution ($T\Delta S$) is observed for all complexes.

The rank order of the binding free energies for the 143D−TMPyP4 complexes is A-4 > A-3 > A-8 > A-2 > A-1 > A-9 > A-7 > A-6 > A-5, and the values of A-6, A-7, and A-5 are significantly smaller than others. The result indicates that the intercalative binding mode has the highest affinity, and next is the end stacking mode. In the intercalative complexes, TMPyP4 is near the center of the quadruplex. The number of the phosphate groups that TMPyP4 can contact is more than that of other complexes, and the TMPyP4 has stacking interactions with two tetrads. In particular, the groove binding complex of A-8 has higher affinity than end stacking complexes. The analysis of the free energy components for A-8 shows that the ΔE_{PBELE} provides favorable contributions to the binding free energy. The rank order of the absolute free energies that can provide a semiquantitative estimate for the stability of the quadruplex−TMPyP4 complexes is: A-8 > A-9 > A-7 > A-1 > A-6 > A-2 > A-5 > A-4 > A-3. The A-8 has the best stability, and next are the external loop stacking complexes of A-9 and A-7. The remaining external binding complexes and the end stacking complexes have similar absolute free energies. The intercalative complexes are most unstable, with significantly smaller values.

The rank order of the binding free energies for the 2KF8−TMPyP4 complexes is B-4 > B-3 > B-2 > B-1 > B-9 > B-5 > B-8 > B-7, and the values of B-9, B-5, B-8, and B-7 are significantly smaller than others. The result also shows that the intercalative binding mode has the highest affinity, and next is the end stacking mode. The rank order of the absolute free energies for the 2KF8−TMPyP4 complexes is: B-1 > B-9 > B-2 > B-8 > B-5 > B-3 > B-7 > B-4. The intercalative complex has the significantly lowest stability. The end stacking complex of B-1 shows the best stability, and next is the external loop binding complex of B-9. All of these findings agree well with the experimental results that TMPyP4 interacts and thermally stabilizes the folded G-quadruplex structures.

PCA. PCA is applied to the backbone atoms of all systems over the last 10 ns simulation. The eigenvalues, which represent the magnitude of the motion, of the first three eigenvectors for all simulation systems are shown in Table 4 and Table 5. The rank order of the eigenvalues for 143D and its complexes is A-3 > A-7 > 143D > A-4 > A-2 > A-1 > A-8 > A-6 > A-5 > A-9, which shows that the eigenvalues of all complexes are much lower than free 143D only except A-3 and A-7. This result confirms that the binding of the TMPyP4 can make the three-tetrad-G-quadruplex structure more rigid almost for all of the modes. Furthermore, the external binding complexes show the highest rigidity, and next are the end stacking complexes. The rank order of the eigenvalues for 2KF8 and its complexes is B-4 > B-3 > B-2 ≫ 2KF8 > B-7 > B-5 > B-9 > B-1 > B-8. The external binding complexes and the end stacking complex of B-1 show higher rigidity than free 2KF8, and the two end stacking complexes of B-3 and B-2 and the intercalative complex of B-4 show very high flexibility. Compared with 143D, 2KF8 has lower eigenvalues and shows higher rigidity. Moreover, the projection of the simulation trajectories onto the planes formed by the first and second principal components for all simulations presents a clear visualization on the phase space

TABLE 5: Eigenvalues (Å^2) of the First Three Eigenvectors for the Two-G-Tetrad Quadruplex and Its Complexes with TMPyP4

	2KF8	B-1	B-2	B-3	B-4	B-5	B-7	B-8	B-9
eigenvector1	20.53	16.95	76.41	102.73	125.90	18.64	20.27	16.91	11.29
eigenvector2	14.58	14.19	34.86	36.09	51.37	10.76	9.22	15.77	7.03
eigenvector2	9.29	8.86	27.11	19.03	22.31	9.11	6.75	10.14	5.42

(Figure S3, Supporting Information). The smaller the phase space is covered, the more rigid the structure is.

Through the above analysis, we can find that the conformation of the antiparallel basket-type two-G-tetrad and three-G-tetrad G-quadruplexes are maintained very well in the presence of K^+ ions during our simulation time with the parm99bsc0 force field. The PCA indicates that 2KF8 is even more rigid than 143D. The two conformations can not be formed simultaneously in the same experimental condition, and so our study complements the experimental data. The TMPyP4 can bind to the G-quadruplexes by several ligand binding modes, namely, end stacking, intercalation, external groove binding, and external loop stacking. The bindings of the end stacking and intercalation are more effective than the external groove binding and external loop stacking. However, not all effective bindings can make the quadruplex structure more rigid and stable.

For the end stacking complexes of A-1, A-2, B-1, B-2, and B-3, the TMPyP4 is stabilized at each site during the whole simulation. The structure analysis indicates that all planes are preserved very well for the five complexes, except the triple1 and triple4 disrupted in the B-2 and B-3, respectively. The free energy analysis indicates that the TMPyP4 can bind to the two quadruplexes effectively by the end stacking mode, with large binding free energies. The PCA shows that the binding of the TMPyP4 at the A-1, A-2, and B-1 sites can make the quadruplexes more rigid, while the binding of the TMPyP4 at the B-2 and B-3 sites causes high flexibility of the quadruplexes, due to the disruption of the triple plane. The analysis of the absolute free energy also shows that A-1, A-2, and B-1 have very good stability. We can see from another viewpoint that B-2 and B-3 also belong to the intercalation mode with the ligand inserted between the tetrad and triple. So we can conclude that the binding sites in the A-1, A-2, and B-1 models are very effective end stacking sites.

For the intercalation complexes of A-3, A-4, and B-4, the TMPyP4 is also stabilized at each site during the whole simulation. The tetrad1 in A-3 and the tetrad2 in B-4 are disrupted to induce the large fluctuation of the rmsd trajectories, while the quadruplex of A-4 is stable with the three tetrads preserved well. Free energy analysis indicates that the intercalation mode has the highest binding affinity compared to other modes but shows the poorest stability. The PCA shows that only the binding of TMPyP4 in the A-4 site can make the G4 more rigid. So we can find that only A-4 is the most possible intercalation mode.

For the external groove binding complexes, the structure analysis shows that the ligands do not reside in the initial grooves. The ligands in the narrow and medium1 grooves of the three-tetrad G-quadruplex are shifted to cap on the A6 base, while the ligands of the two-tetrad G-quadruplex tend to leave the quadruplex. The displacements of the ligands in the wide and medium2 grooves are small, and the interactions between the TMPyP4 and the quadruplexes are mainly by the electronic attraction between the pyridinium groups and phosphate groups. Free energy analysis indicates that the external bindings are significantly weaker than others, but the stability of the complexes is relatively high. The PCA indicates that only the eigenvalue of A-7 is larger than that of the free quadruplex. The ligands in the external loop stacking complexes of A-9 and B-9 have the stacking interactions with the lateral loop bases. Their binding free energies are between the end stacking complexes and the grooving binding complexes, and the stability of the two complexes is very high. The PCA analysis shows that the binding of TMPyP4 in the A-9 and B-9 sites can make the G4 more rigid. So, the external loop stacking mode is also very favorable.

Conclusively, the end stacking mode of A-1, B-1, and A-2 is the best, with high binding affinity and high stability of quadruplexes, and next is the external loop stacking mode of A-9 and B-9, with relatively high affinity and high stability and the intercalation mode of A-4, with very high affinity and relatively high stability. The remaining external binding complexes have relatively low affinity and high stability, which are superior to end stacking complexes of B-2 and B-4 and the intercalation complexes of A-3 and B-4, showing very high affinity and high flexibility. The sites that can stabilize the three-G-tetrad G-quadruplex structure are more than the two-G-tetrad G-quadruplex in the range of our investigation. The external binding sites provided in our paper are not the entirety, but they can be used as a representative to show the characteristics of the nonspecific external binding mode. We find that the external binding sites are random and the number is many, which can explain the experimental phenomenon that the binding stoichiometry of TMPyP4 to human telomeric quadruplex structures increases with the TMPyP4 addition.

Many studies were reported on the end stacking and intercalation binding modes of TMPyP4 with other G-quadruplex DNA. For example, Freyer et al. reported that the binding of TMPyP4 to the *c-myc* NHE III promoter is in the ratio of 4:1 and shows two binding modes of end stacking and intercalation, using microcalorimetric and spectroscopic techniques and molecular modeling.[44] Nagesh et al. proposed that TMPyP4 can bind externally as well as intercalate between the two G-tetrads of quadruplex DNA formed by the promoter region of *c-myc* and Bcl2 oncogenes, based on CD, fluorescence, and UV−vis spectroscopic techniques.[45] In my study, the end stacking mode of A-1, B-1, and A-2 is a very favorable binding mode, and only the intercalation mode of A-4 is favorable. The rest of the intercalation complexes have high flexibility and poor stability. Two G-tetrads capping on top of the TMPyP4 and one G-tetrad, one triple, and loop bases below the TMPyP4 produce large stacking interactions, which is the reason for the A-4 with relatively high stability. Cavallari et al. also found that the possibility of regular TMPyP4 intercalation depends on the length of the quadruplex.[31]

The differences in affinity of "end stacking" vs "intercalation" interactions in my study is about 10 kcal/mol, which is larger than the difference of less than 2 kcal/mol between TMPyP4 and *c-myc* in the experimental finding.[44] The MM-PBSA approach developed by Kollman and Case[46,47] has become a popular method for estimating binding affinities of biomolecular complexes, but the method is slightly less accurate and is not able to predict binding free energies in quantitative agreement with the experimental values. The greatest source of error in the absolute binding free energy is the solute entropy term because estimates of entropy from normal-mode analysis have

some limitations. Nevertheless, many published application examples indicated that calculated and experimental free energies of binding were significantly correlated.[48] Our aim of free energy calculations is to make comparisons among different binding modes and provide a semiquantitative estimate of quadruplex model stability and binding affinity with the ligands, not to compare quantitatively with the experimental values.

Previous molecular modeling work on quadruplex−TMPyP4 complexes only studied one or two kinds of binding modes, and they did not perform long MD simulations to validate the stability of the conformations or compute and compare the binding free energies of the complexes and the affects of the binding of TMPyP4 to the flexibility of the quadruplex structures.[15,16,49] In my work, we carry out extended MD simulations to investigate almost all binding modes, which samples conformational phase spaces sufficiently. The detailed structure analysis, free energy calculations, and PCA are performed to validate the stability of conformations and compare the binding affinity among conformations and the dynamic affect of ligand binding to the quadruplexes.

Conclusions

Two basket-type G-quadruplexes with the sequence of d[$(GGGTTA)_3GGG$] and their complexes with TMPyP4 are investigated by a combination of molecular modeling and molecular dynamic simulation methods in water with the existence of K^+ ions in the central channel. We show the 3D structures of the G-quadruplex−TMPyP4 complexes with almost all possible binding modes. The detailed structure analysis, free energy calculations, and principal components analysis show that the end stacking mode of A-1, B-1, and A-2 is the best, and next are the external loop stacking mode of A-9 and B-9 and the intercalative mode of A-4. The remaining external binding complexes are superior to the end stacking complexes of B-2 and B-4 and the intercalation complexes of A-3 and B-4. The sites that can stabilize the three-G-tetrad G-quadruplex structure are more than the two-G-tetrad G-quadruplex. Our investigation will assist in understanding the binding interactions of TMPyP4 with the antiparallel human telomeric G-quadruplexes and may be helpful as a platform for rational drug design.

Acknowledgment. This work was supported by the National Science Foundation of China (20973049, 20673044), PCSIRT (IRT0625). We would like to thank professor David A. Case et al. for giving us the Amber 10.0 software as a freeware.

Supporting Information Available: Plots of rmsd vs time and plots of the planes of the first and second principal components. This material is available free of charge via the Internet at http://pubs.acs.org.

References and Notes

(1) Moyzis, R. K.; Buckingham, J. M.; Cram, L. S.; Dani, M.; Deaven, L. L.; Jones, M. D.; Meyne, J.; Ratliff, R. L.; Wu, J. R. *Proc. Natl. Acad. Sci. U.S.A.* **1988**, *85*, 6622.

(2) Wright, W. E.; Tesmer, V. M.; Huffman, K. E.; Levene, S. D.; Shay, J. W. *Genes Dev.* **1997**, *11*, 2801.

(3) Chen, F. M. *Biochemistry* **1992**, *31*, 3769.

(4) Henderson, E.; Hardin, C. C.; Walk, S. K.; Tinoco, I., Jr.; Blackburn, E. H. *Cell* **1987**, *51*, 899.

(5) Williamson, J. R.; Raghuraman, M. K.; Cech, T. R. *Cell* **1989**, *59*, 871.

(6) Zahler, A. M.; Williamson, J. R.; Cech, T. R.; Prescott, D. M. *Nature* **1991**, *350*, 718.

(7) Kim, N. W.; Piatyszek, M. A.; Prowse, K. R.; Harley, C. B.; West, M. D.; Ho, P. L.; Coviello, G. M.; Wright, W. E.; Weinrich, S. L.; Shay, J. W. *Science* **1994**, *266*, 2011.

(8) Read, M. A.; Neidle, S. *Biochemistry* **2000**, *39*, 13422.

(9) Randazzo, A.; Galeone, A.; Luciano, M. *Chem. Commun.* **2001**, *11*, 1030.

(10) Clark, G. R.; Pytel, P. D.; Squire, C. J.; Neidle, S. *J. Am. Chem. Soc.* **2003**, *125*, 4066.

(11) Haider, S. M.; Parkinson, G. N.; Neidle, S. *J. Mol. Biol.* **2003**, *326*, 117.

(12) Wheelhouse, R. T.; Sun, D.; Han, H.; Han, F. X.; Hurley, L. H. *J. Am. Chem. Soc.* **1998**, *120*, 3261.

(13) Parkinson, G. N.; Ghosh, R.; Neidle, S. *Biochemistry* **2007**, *46*, 2390.

(14) Mita, H.; Ohyama, T.; Tanaka, Y.; Yamamoto, Y. *Biochemistry* **2006**, *45*, 6765.

(15) Han, H.; Langley, D. R.; Rangan, A.; Hurley, L. H. *J. Am. Chem. Soc.* **2001**, *123*, 8902.

(16) Haq, I.; Trent, J. O.; Chowdhry, B. Z.; Jenkins, T. C. *J. Am. Chem. Soc.* **1999**, *121*, 1768.

(17) Wei, C.; Jia, G.; Yuan, J.; Feng, Z.; Li, C. *Biochemistry* **2006**, *45*, 6681.

(18) Zhang, H. J.; Wang, X. F.; Wang, P.; Ai, X. C.; Zhang, J. P. *Photochem. Photobiol. Sci.* **2008**, *7*, 948.

(19) Gaynutdinov, T. I.; Neumann, R. D.; Panyutin, I. G. *Nucleic Acids Res.* **2008**, *36*, 4079.

(20) Martino, L.; Pagano, B.; Fotticchia, I.; Neidle, S.; Giancola, C. *J. Phys. Chem. B* **2009**, *113*, 14779.

(21) Wang, Y.; Patel, D. J. *Structure* **1993**, *1*, 263.

(22) Lim, K. W.; Amrane, S.; Bouaziz, S.; Xu, W.; Mu, Y.; Patel, D. J.; Luu, K. N.; Phan, A. T. *J. Am. Chem. Soc.* **2009**, *131*, 4301.

(23) Phan, A. T.; Kuryavyi, V.; Gaw, H. Y.; Patel, D. J. *Nat. Chem. Biol.* **2005**, *1*, 167.

(24) *INSIGHTII; Modelling EnVironment*; Molecular Simulations Inc. (MSI), 1984.

(25) Cavallari, M.; Calzolari, A.; Garbesi, A.; Di Felice, R. *J. Phys. Chem. B* **2006**, *110*, 26337.

(26) Guschlbauer, W.; Chantot, J. F.; Thiele, D. *J. Biomol. Struct. Dyn.* **1990**, *8*, 491.

(27) Hardin, C. C.; Watson, T.; Corregan, M.; Bailey, C. *Biochemistry* **1992**, *31*, 833.

(28) Xu, Q.; Deng, H.; Braunlin, W. *Biochemistry* **1993**, *32*, 13130.

(29) Case, D. A.; Darden, T. A.; Cheatham, T. E., III; Simmerling, C. L.; Wang, J.; Duke, R. E.; Luo, R.; Crowley, M.; Ross, W. C.; Zhang, W.; Merz, K. M.; Wang, B.; Hayik, S.; Roitberg, A.; Seabra, G.; Kolossváry, I.; Wong, K. F.; Paesani, F.; Vanicek, J.; Wu, X.; Brozell, S. R.; Steinbrecher, T.; Gohlke, H.; Yang, L.; Tan, C.; Mongan, J.; Hornak, V.; Cui, G.; Mathews, D. H.; Seetin, M. G.; Sagui, C.; Babin, V.; Kollman, P. A. *AMBER 10*; University of California: San Francisco, CA, 2008.

(30) Wang, J.; Wolf, R. M.; Caldwell, J. W.; Kollman, P. A.; Case, D. A. *J. Comput. Chem.* **2004**, *25*, 1157.

(31) Cavallari, M.; Garbesi, A.; Di Felice, R. *J. Phys. Chem. B* **2009**, *113*, 13152.

(32) Lubitz, I.; Borovok, N.; Kotlyar, A. *Biochemistry* **2007**, *46*, 12925.

(33) Price, D. J.; Brooks, C. L. *J. Chem. Phys.* **2004**, *121*, 10096.

(34) Thenmalarchelvi, R.; Yathindra, N. *Nucleic Acids Res.* **2005**, *1*, 43.

(35) Darden, T.; Perera, L.; Li, L.; Pedersen, L. *Structure* **1999**, *7*, R55.

(36) Hauptman, H. A. *Methods Enzymol.* **1997**, *277*, 3.

(37) Perez, A.; Marchan, I.; Svozil, D.; Sponer, J.; Cheatham III, T. E.; Laughton, C. A.; Orozco, M. *Biophys. J.* **2007**, *92*, 3817.

(38) Luo, R.; David, L.; Gilson, M. K. *J. Comput. Chem.* **2002**, *23*, 1244.

(39) Sitkoff, D.; Sharp, K. A.; Honig, B. *J. Phys. Chem.* **1994**, *98*, 1978.

(40) Fadrna, E.; Spackova, N.; Stefl, R.; Koca, J.; Cheatham, T. E.; Sponer, J. *Biophys. J.* **2004**, *87*, 227.

(41) Haider, S.; Parkinson, G. N.; Neidle, S. *Biophys. J.* **2008**, *95*, 296.

(42) Amadei, A.; Linssen, A. B.; Berendsen, H. J. *Proteins* **1993**, *17*, 412.

(43) Kitao, A.; Go, N. *Curr. Opin. Struct. Biol.* **1999**, *9*, 164.

(44) Freyer, M. W.; Buscaglia, R.; Kaplan, K.; Cashman, D.; Hurley, L. H.; Lewis, E. A. *Biophys. J.* **2007**, *6*, 2007.

(45) Nagesh, N.; Sharma, V. K.; Ganesh Kumar, A.; Lewis, E. A. *J. Nucleic Acids* **2010**, doi:10.4061/2010/146418.

(46) Kollman, P. A.; Massova, I.; Reyes, C.; Kuhn, B.; Huo, S.; Chong, L.; Lee, M.; Lee, T.; Duan, Y.; Wang, W.; Donini, O.; Cieplak, P.; Srinivasan, J.; Case, D. A.; Cheatham, T. E., Jr. *Acc. Chem. Res.* **2000**, *33*, 889.

(47) Wang, J.; Morin, P.; Wang, W.; Kollman, P. A. *J. Am. Chem. Soc.* **2001**, *123*, 5221.

(48) Ferrari, A. M.; Degliesposti, G.; Miriam, S.; Rastelli, G. *Bioorg. Med. Chem.* **2007**, *15*, 7865.

(49) Cashman, D. J.; Buscaglia, R.; Freyer, M. W.; Dettler, J.; Hurley, L. H.; Lewis, E. A. *J. Mol. Model.* **2008**, *14*, 93.

JP101373P